Original Paper

Highly reflective subtractive color filters capitalizing on a silicon metasurface integrated with nanostructured aluminum mirrors

Wenjing Yue[1], S[illegible] Gao[1], Sang-Shin Lee[1,*], Eun-Soo Kim[1], and Duk-Yong Choi[2]

[*]Correspondi[illegible]lee@kw.ac.kr

[1]Department of Electronic Engineering, Kwangwoon University, 20 Kwangwoon-ro, Nowon-gu, Seoul 01897, South [illegible]

[2]Laser Physics Centre, Research School of Physics and Engineering, Australian National University, Canberra ACT 2601, Australia

Abstract

Metasurface-based color filters have been recently applied for the creation of imaging devices and color printing in a sub-wavelength scale. In this work, a highly reflective subtractive color filter featuring an excellent color contrast is conceived and demonstrated, by exploiting a crystalline-silicon nanopillar (NP)-based dielectric metasurface integrated with an aluminum disk mirror (DM) and holey mirror (HM) at the top and bottom, respectively. A deep suppression in reflection is acquired through magnetic dipole (MD) resonance that is supported by the constituent NP, and can be effectively tailored via the control of the NP diameter. The cooperation of the nanostructured DM and HM plays a dual role of dramatically boosting the efficiency and reinforcing the confinement of the MD of the NP, which is primarily accountable for the reduction in the spectral bandwidth. For the manufactured filters, both a high reflection efficiency reaching ~70% and relatively small bandwidth of ~55 nm are attained, thus leading to a broad palette of vivid and bright colors. The proposed devices are supposed to exhibit a polarization-insensitive operation and a relaxed angular tolerance, thereby facilitating the implementation of miniaturized display/imaging devices with a high resolution and excellent color fidelity.

Graphical Abstract Highly reflective subtractive color filters featuring an excellent color contrast is conceived and demonstrated, by taking advantage of a crystalline-silicon nanopillar (NP)-based dielectric metasurface integrated with an aluminum disk mirror and holey mirror at the top and bottom, respectively. The reflection dip can be effectively tailored via the control of the NP diameter, thus leading to the output subtractive colors of cyan, magenta and yellow.

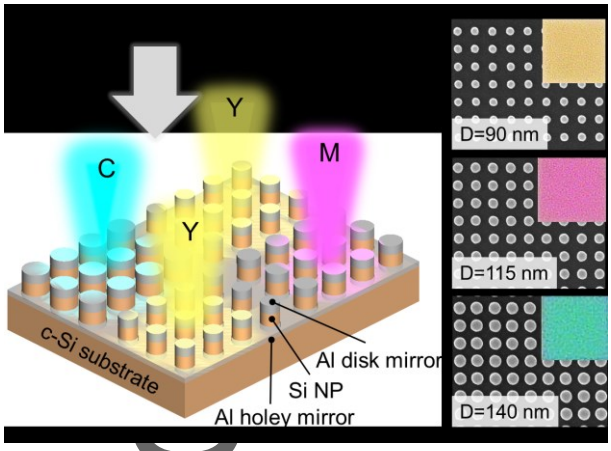

Key words:

Structural colors, silicon metasurfaces, Mie resonances, nanoresonators, metallic thin films

1. Introduction

Structural color filters, which are mediated by the interaction between incident visible light and nanostructures instead of the inherent properties of materials, have received a burgeoning amount of interest in the fields of photorealistic color printing, plastic consumer products, color holograms, anti-counterfeiting, among others.[1-8] Compared with the conventional toxic dye/pigment-based colorants, the structural filters deliver conspicuous merits encompassing the cost effectiveness, environment friendliness, high reproduction fidelity and sustainability. Inspired by the photonic structures discovered in nature, such as the wings of Morphobutterflies,[9,10] multi-layered nanostructures, diffraction gratings and metasurfaces were chiefly exploited to realize a wide range of structural colors.[11-27] Such artificially engineered nanophotonic structures are useful for manipulating the spectral properties of transmission, reflection, and absorption in the visible spectral regime via the modification of their design parameters. However, the configuration of the

multiple layers is not adequate for generating a complicated color pattern in a small scale in view of the precision multi-step lithography processes that are required to produce different colors, on top of the difficulty in the thickness control.[11-15] For the nanostructures resorting to the diffraction grating, a severe angular dependence is likely to emerge due to the dependence of its spectral resonance on the periodicity,[16-18] which poses a grave concern for the applications like the imaging and color printing. Moreover, the pixel size is fundamentally tightly limited.

From the perspective of concocting both high-resolution imaging/display devices and color printing devices in a subwavelength scale, a metasurface, which refers to a nanostructured functional plane that is constructed by an array comprised of periodically arranged meta-atom building blocks, such as plasmonic nanostructures and high-index nanoparticles,[28,29] gained abundant attention as a prominent color filtering device due to its conspicuous features, including downscaled color printing beyond the diffraction limit, simplified fabrication process, and angular insensitivity.[19-27] By tailoring the geometry of the unit resonators and their arrangement, the optical reflection/transmission spectra are adaptively controlled in the visible band thus render various color outputs. Silicon (Si), which is the second-most-abundant material in nature and the most prevalent material in the semiconductor industry, is advantageous in terms of its low cost, full compatibility with complementary metal-oxide-semiconductor process, and ease of fabrication. In view of its high refractive index of n = ~4.0, Si is regarded as an eminent candidate for constructing a variety of metasurface. Recently, several reflection type structural color filters were reported based on Si, which can readily integrate into other optical/electrical devices.[25-27,30-32] The approach that taps into a Si metasurface is anticipated to exhibit a good stability and compactness,[25-27] compared with the conventional Si nanowires of an extremely high aspect ratio.[30-32] For the

transmission-type filter based on a Si metasurface, it can provide higher efficiency beyond 90% than its plasmonic counterpart, which suffers from high conduction loss in the visible band.[33,34] However, a reflection-type filter, which capitalizes on Si metasurfaces formed on a Si substrate,[25-27] may exhibit lower efficiency compared to its plasmonic counterpart,[3,6,20,24] due to the low reflectivity of Si. It is resultantly evident that the crosstalk worsens while the color contrast is degraded. Here, the color contrast, which pertains to the brightness as well as the chromatic color that corresponds to the purity of color as observed at a constant level of brightness, may be adequately used to give insight into the relationship between the chromaticity coordinates of colors and their perception.[35] It is noted that a reflection spectrum that exhibits a high extinction ratio between the off-resonance efficiency and resonance dip, in conjunction with a small bandwidth leads to a high color contrast.[1,21]

In this paper, reflective subtractive color filters, which enable an enhanced efficiency and excellent color contrast, have been proposed and built by capitalizing on a crystalline-silicon (c-Si) nanopillar (NP)-based metasurface that is integrated with a nanostructured disk mirror (DM) and holey mirror (HM) in aluminum (Al) at the top and bottom, respectively. The constituent Si NP resonators are individually utilized to resonantly excite a magnetic dipole (MD) that is mediated by the Mie scattering. The mode associated with the MD resonance can efficiently couple to the Si substrate of a high index, giving rise to a pronounced near-zero dip in reflection. This reflection dip can be effectively tuned via the adjustment of the NP diameter. The nanostructured DM and HM cooperatively play a dual role of considerably boosting the off-resonance reflection and elevating the confinement of the MD in the NP, which is keenly related to an appropriate reduction in the spectral bandwidth. A set of devices were prepared to confirm the claimed performance,

encompassing a high reflection, good color contrast, wide color tunability throughout the visible band. Lastly, the mechanism underlying the resonance dip and the role originating from the cooperation of the two nanostructured mirrors were meticulously investigated through the inspection of the electric (E) and magnetic (H) field profiles.

2. Experimental materials and methods

2.1. Device fabrication

Considering Al and Si are commonly used materials in the semiconductor industry, the fabrication of the proposed filter device was facilitated by adopting a series of standard processes, including electron beam lithography (EBL), silicon plasma etching, and Al deposition via electron beam evaporation. The detailed fabrication procedure is described as follows. A holey film that is made of a positive electron-beam resist of ZEP520A was initially patterned on a single c-Si wafer with an EBL system (RAITH 150). A 55-nm thick Al film was subsequently deposited with an electron-beam evaporator (Temescal BJD-2000 E-beam Evaporator system). When the resist was completely removed via a lift-off process by means of a ZEP remover (ZDMAC), a square lattice of Al disks was made on the substrate. By utilizing the Al disk pattern as a hard mask, the substrate was dry etched in a plasma etcher (ICP-RIE Plamalab100 from Oxford) that resorts to a mix of CHF3 and SF6 gases, thereby constructing a Si NP with a height of 180 nm. During the Si plasma etching the Al layer was practically eroded by 5 nm. A 10-nm thick Al layer was similarly deposited with an electron-beam evaporator. Consequently, a DM and HM of 60-nm and 10-nm heights were created at the top and bottom, respectively. By ensuring a high vacuum of as low as 0.001 Pa and a long mean-free-path for

the Al plume during the evaporation, a directional film deposition was promoted to guarantee that the sidewall of the Si NP is rarely exposed to the Al deposition. The completed color filters assume dimensions of 30 μm × 30 μm. It is known that the EBL is only suitable for small-scale nano-patterning due to its long writing time. Nanoimprinting[36] or laser interference lithography[37] may be potentially considered for manufacturing a large-scale version of the proposed color filters.

2.2. Simulations

Full-field electromagnetic wave simulations were fulfilled for the design of proposed filter with the assistance of a tool based on the finite difference time domain (FDTD) method (FDTD Solutions, Lumerical, Canada).[38] The dispersion characteristics of Al and Si used for the simulations, as plotted in Figure S1 in the supporting information, were derived from the multi-coefficient model offered by the simulation tool. A plane wave served as a light source.

2.3. Optical characterization

The scanning electron microscope (SEM) images of the fabricated color filters were taken under a high-resolution SEM (S-4800, Hitachi). The optical reflection was measured under the normal incidence using a spectroscopic reflectometer (Elli-Rsc, Ellipso Technology). The measurement of the reflection spectra as a function of the incident angle was carried out through an angle-resolved microspectroscopy system (ARM available from ideaoptics, China).

3. Results and discussion

3.1. Proposed highly efficient subtractive color filters and their performances

Figure 1(a) illustrates the schematic configuration of the proposed structural color filters, which produces three primary subtractive colors of cyan, magenta, and yellow (CMY). Each of the filters is based on a metasurface incorporating a c-Si NP array that is integrated with an Al DM at the top and an Al HM at the bottom, which is formed on a similar Si substrate. The heights of the top DM, NP, and bottom HM are denoted by H_1, H_2, and H_3, respectively. A multitude of NPs of a diameter D are arranged in a square lattice in accordance with a period P. For normally incident light, the polarization is indicated by an angle ϕ of the E-field with respect to the x-direction. The impinging light may resonantly couple to the NPs in association with the Si metasurface, thus introducing a strong wavelength-selective suppression in the reflection spectra. Such a reflection dip can be scanned across the entire visible spectral regime through the control of the NP diameter, thus providing a vivid color output. A plasmonic color filter has been reported by introducing a low-index dielectric material rather than Si for the NPs between two nanostructured metallic layers.[21] The plasmonic device resorts to a surface plasmon resonance associated with metal-dielectric interfaces. Meanwhile, the proposed color filter dominantly relies on the Mie resonance instead of the plasmonic resonance, which is efficiently mediated by a dielectric metasurface comprising an array of high-index Si NPs. A detailed analysis of the mechanism for the proposed filter will be described later. It is remarked that for the proposed device, color filtering can be achieved even in the absence of nanostructured metallic mirrors.

By optimizing the proposed structure by virtue of rigorous simulations, the NP array has been chosen to have a period of 240 nm so that a near-zero dip in reflection could be obtained by resonantly coupling the incident light to the proposed structure via the Mie scattering mediated by the NP array. The height of Si NP is properly determined to be H_2 = 180 nm so as to ensure that only

a single near-zero reflection dip occurs in the visible spectral band. The determination of the height for the Al DM and HM is elaborated in Figures S2(a) and S2(b) in the supporting information. The reflection spectra of the filter are observed to remain stable in terms of the location of resonance dip and the reflection efficiency in the case of an Al DM with a height ranging from H_1 = 20 to 80 nm. For the Al HM, the height is to be below 30 nm so as to prevent the appearance of an unwanted reflection dip at λ = 660 nm, which results from the strong coupling between the localized surface plasmon resonances in connection with the top Al DM and the bottom Al HM,[4,19] as observed in the field profiles shown in Figure S2(c) in the supporting information. Finally, the heights of the top Al DM and the bottom Al HM were determined to H_1 = 60 nm and H_3 = 10 nm, respectively, thereby boosting the off-resonance reflection. A group of devices that is responsible for the CMY colors were cultivated and assessed. The fabrication procedure adopted for the device is shown in Figure 1(b), which is expounded in the Experimental materials and methods.

Figure 2(a) shows the SEM images of the completed CMY color filters, having NP diameters of D = 90 , 115 , and 140 nm for a period of P = 240 nm. The heights of the Al DM, Si NP, and Al HM were respectively measured to be H_1 = 60 nm, H_2 = 180 nm, and H_3 = 10 nm, as intended. It is observed from the top view of the fabricated device that well-defined circular patterns are periodically arranged in a square lattice, exhibiting a high fidelity to the design. The side view indicates, however, that the Si NPs are found to exhibit slightly slanted sides due to imperfect etching, while the top Al DM is slightly rounded. It was found through simulations that the reflection spectra are negligibly sensitive to the shape of the Al DM while a small resonance shift is incurred by the slanted sides of the NPs. As a result, the simulations based on the ideal structures of the Al DM and Si NP are surely reliable. The bright-field microscope images pertaining to the generated colors of yellow, magenta

and cyan, with dimensions of 30 μm × 30 μm, are included in the inset of Figure 2(a), rendering an enhanced contrast. The reflection spectra were inspected under the normal incidence using a spectroscopic reflectometer (Elli-Rsc, Ellipso Technology) and compared with the simulation results, as shown in Figure 2(b). Decent correlations were attained between the measured and simulated reflection spectra in terms of the efficiency and the location of the resonance dips. The spectra were monitored to exhibit a drastic suppression in reflection at the resonance wavelengths of 489 nm, 552 nm, and 609 nm, corresponding to the desired subtractive colors of yellow, magenta, and cyan, respectively. A high off-resonance reflection surpassing 70% alongside a relatively narrow full-width-at-half-maximum bandwidth of ~55 nm was achieved, which is noteworthy compared with the previous approaches that rely on a Si nanostructure, where the spectra are inclined to exhibit multiple resonance dips in the visible band or give a low reflection below 40%.[26,27,30] To estimate the color purity at a given brightness, the related chromaticity coordinates were calculated from the simulated and the measured spectra and then mapped on the standard International Commission on Illumination (CIE) 1931 chromaticity diagram, as shown in Figure 2(c).

For the proposed filters, a broad palette of subtractive colors can be created by altering the NP diameter and hence tuning the resonance wavelength. Toward that end, a set of devices with different NP diameters ranging from D = 90 to 160 nm were fabricated for a fixed period of P = 240 nm. Figure 3(a) shows the reflection spectra, wherein the resonance dip is observed to progressively red shift from λ = 489 to 660 nm, as indicated by the dashed lines. The insets contain the optical microscope images available from the devices, featuring a vivid color that runs from yellow to green. In a bid to verify the impact of the nanostructured DM and HM on the spectra and relevant colors, the case of a NP array with no mirror applied was studied. Figure S3(a) in the supporting information

deals with a comparison of the spectra between the cases with and without the nanostructured metallic mirrors. The proposed device that taps into the mirrors leads to an approximate increase of 50% in the off-resonance reflection while the spectral bandwidth is substantially narrowed. The notable increase in the reflection is mainly attributed to the elevated reflectivity that is empowered by the cooperation of the DM and HM, which covers the whole surface of the Si metasurface. The proposed filters are hence able to generate a vivid color as well as a large color gamut, which can be verified by probing the optical microscope images pertaining to the two structures, as shown in Figures 3(a) and S3(b). As plotted in Figure 3(b), the relevant chromaticity coordinates in the CIE 1931 chromaticity diagram are observed to evolve along the black arrow with increasing NP diameter.

The reflection spectra in terms of the period of the NP array was then explored, as shown in Figure S4(a) in the supporting information. The near-field coupling between two adjacent NPs was numerically calculated to decline as the period of the NP array increases, resulting in a slight red shift of the resonance wavelength, as shown in Figure S4(a) in the supporting information. This has been proved by monitoring the E-field profiles at resonance when the NP is altered in period for a fixed diameter, as shown in Figure S4(b) in the supporting information. Figure S4(c) in the supporting information shows the reflection spectra of the proposed structure with the NP diameter, which ranges from D = 75 to 150 nm, for a NP-to-NP gap of 100 nm. A linear relationship arises between the resonance wavelength and the NP diameter, which can be applied to estimate the resonance wavelength. Besides, as shown in Figure S5 in the supporting information, the proposed filters are deemed to enable polarization-independent performance for the normal incidence, which is attributed to the symmetrical geometry of the proposed structures.[16] Figure 4(a) shows the

simulated reflection spectra of the magenta filter with respect to the incident angle θ for the transverse-magnetic (TM) and transverse-electric (TE) polarizations corresponding to $\phi = 0^{o}$ and $\phi = 90^{o}$, respectively. The resonance dip is observed to be stably preserved for the angles ranging up to 25^{o} and 30^{o} for the TM and TE polarizations, respectively, signifying a relaxed angular tolerance. In order to facilitate the measurement of the angular dependence, a set of CMY filters with sufficiently large dimensions (300 μm × 300 μm) were additionally fabricated based on the same design parameters as mentioned before. The measured reflection spectra for the normal incidence are shown in Figure S6 in the supporting information, which fairly resembles the results shown in Figure 2b. Especially for the newly prepared magenta filter, the reflection spectra with the incident angle were checked for the TM and TE polarizations as shown in Figure 4(b). The resonance dip is witnessed to be stably preserved for the angles ranging up to 25^{o} and 30^{o} for the TM and TE polarizations, respectively, thereby rendering a good correlation between the simulation and measurement results. The mechanism underlying the angle-insensitivity will be elaborated later. The observed polarization independence and relaxed angular tolerance make the proposed filters suitable for their potential applications in the color displays, imaging, and color printing.

3.2. Mechanism underlying the reflection dip and role of the pair of Al DM and HM

In an attempt to expound the mechanism underlying the wavelength-selective reflection dips, we rigorously inspected the E- and H-field profiles at resonance in the case of the magenta device. For a metasurface that involves an array of Si NPs, each NP acts as a resonator, which allows for the excitation of the MD and electric dipole (ED) resonance modes in the visible spectral band.[33,34,39,40] A strong MD resonance is indicated by a displacement current loop inside of the Si NP, which corresponds to an antiparallel E-field polarization in the proximity of either boundary of

the NP. Considering it is induced in accordance with the effective wavelength in the Si NP, the MD resonance would be efficiently tuned through the adjustment of the NP diameter. By tethering an array of Si NPs to a high-index substrate of the same material, the light stored in the mode that is confined in the NP resonator can preferentially resonantly couple to the high-index substrate, thus bringing about a significantly suppressed reflection. As shown in Figure 5(a), for the magenta filter with the NP diameter of D = 115 nm, the simulated reflection assumes a resonance dip exhibiting a near-zero reflection at λ = 552 nm. With the intention of exploring the resonance pertaining to the reflection dip, the E- and H-field profiles are plotted in the x-z plane in Figure 5(b). A reinforced circular E-field trajectory, as marked by the black arrow, develops within the Si NP so that a displacement current loop forms, while a strengthened H-field is concurrently produced in the out-of-plane direction. Apparently, the presence of the MD resonance is accordingly excited. It is noted that the E-field is locally enhanced around the Al DM while a strong E-field loop develops in the Si NP at resonance. Rigorous simulations supported that the field enhancements inside of the Si NP and around the Al DM transpire simultaneously for the proposed structure with Al mirrors and the case without Al mirrors;[26,39,40] The field enhancement vanishes at off-resonance for the two cases. In addition, the plasmon resonances that may be possibly supported by the proposed structure are found to play no significant role in the visible spectral band, as described in the supporting information with the help of Figure S7. It is resultantly inferred that the strengthened E-field around the Al DM may be related to the Mie scattering-induced MD resonance concomitant with the Si NP, instead of the surface plasmon resonance. By thoroughly scrutinizing the field profiles, we could conclude that the reflection dip is categorically dominated by the MD resonance that is supported by the Si NP. It is noted that for the NP diameters exceeding 130 nm, a new resonance dip is found to

appear at a shorter wavelength, as shown in Figure 3(a). The dip is thought to be induced by a higher-order mode of Mie resonance, which is equivalent to the magnetic quadrupole mode,[40,41] as confirmed through the field profiles at resonance. In order to understand the mechanism underpinning the angular insensitivity, for the magenta filter, the normalized E- and H-field profiles at resonance has been inspected for the incident angles of $\theta = 25^{o}$ and 30^{o} for the TM and TE polarizations, respectively, as shown in Figure S8(a) in the supporting information. A well-defined MD resonance mode is concretely observed for the NPs for both polarizations as in the case of the normal incidence, signifying that the structure invoking the Mie scattering is verified to enable a relaxed angular tolerance, as intended.[42] For comparison, the simulated field profiles for the structure with no Al mirrors have also been investigated as shown in Figure S8(b).

We undertook the task of investigating the behavior of the nanostructured metallic DM and HM that are incorporated into the proposed color filter. In this respect, four different structures, which include the cases of no Al mirror, an Al DM, an Al HM, and a combination of the DM and HM, were comparatively assessed in terms of the reflection response, as plotted in Figure 6(a). For the case with no Al mirror, the reflection spectrum features a broad bandwidth in tandem with a low off-resonance efficiency, resulting in a dim color with low contrast, as shown in Figure S3(b) in the supporting information. The poor off-resonance reflection might be imputed to the low reflectivity of Si as aforementioned. For the cases engaging either the DM or HM, a nearly two-fold efficiency enhancement could be realized, yet the off-resonance efficiency rises barely up to 40%, which is by far below that for the case that relies on an optically thick metallic substrate.[3,6,20,24] For the proposed filter engaging the DM-HM pair, the off-resonance reflection is substantially boosted, while the spectral bandwidth is drastically diminished, thereby obtaining a high color contrast. To

have an insight into the variations in the bandwidth, the E- and H-field profiles in the x-z plane are monitored for the above four structures, as shown in Figure 6(b). The existence of a circular E-field loop and an excited MD resonance mode were concretely validated in relation to the Si NP for the four different structures. For the typical case with no mirror, the resonance mode was discovered to be weakly confined by the NP while the relating field appreciably spreads to the high-index substrate of Si. Consequently, the NP resonator manages to assume a broad spectral bandwidth, equivalent to a low quality factor. In contrast to the structure with no mirror, the proposed configuration gives rise to a noticeable field enhancement in conjunction with a considerably strengthened mode confinement within the NP, which translates into a high quality factor.

4. Conclusions and outlook

A group of reflective subtractive color filters that permit enhanced color contrast were successfully presented by resorting to a c-Si NP-based dielectric metasurface, which is combined with a pair of metallic nanostructures of DM and HM. For the metasurface, an efficient MD resonance was revealed to be individually supported by a NP element, accounting for a pronounced resonance dip in the reflection spectra. The reflection dip could be effectively tuned over the whole visible band through the adjustment of the NP diameter. The cooperation of the nanostructured DM and HM played a dual role of raising the reflection efficiency at off-resonance and markedly promoting the confinement of the MD mode in the Si NP, which was validated based on the reduced spectral bandwidth. A group of filter devices with different NP diameters were prepared to prove the claimed performances including an off-resonance reflection of up to 70%, a modest spectral bandwidth of ~55 nm, and a broad palette of bright colors that permits a high contrast and extended gamut. The proposed color filters are anticipated to give rise to both a relaxed angular tolerance and

polarization independence to a certain extent. They are capable of categorically facilitating the development of ultra-compact display/imaging devices that enable a high resolution and excellent color fidelity.

Supporting Information

Additional supporting information may be found in the online version of this article at the publisher's website.

Figure S1: Dispersion characteristics of c-Si and Al materials.

Figure S2: Determination of the heights of Al DM and Al HM

Figure S3: Influence of the nanostructured Al mirrors on the performances of the proposed color filters.

Figure S4: Dependence of the reflection dip on the period and the diameter of NPs.

Figure S5: Performance of the proposed filter hinging on the polarization.

Figure S6: Measured reflection spectra for the additionally prepared CMY filters with larger dimensions.

Figure S7: Investigation of the plasmonic effect for the proposed structure.

Figure S8: Mechanism behind the angle-insensitive property of the proposed filter.

Acknowledgements

This work was supported by a National Research Foundation of Korea (NRF) grant funded by the Korea government (MSIP) (No. 2016R1A2B2010170 and 2011-0030079) and by the Research Grant of Kwangwoon University in 2017. The work was partly supported by the Australian Research Council

Future Fellowship (FT110100853, Dr. Duk-Yong Choi) and was performed in part at the ACT node of the Australian National Fabrication Facility.

Received: ((will be filled in by the editorial staff))
Revised: ((will be filled in by the editorial staff))
Published online: ((will be filled in by the editorial staff))

References

[1] S. J. Tan, L. Zhang, D. Zhu, X. M. Goh, Y. M. Wang, K. Kumar, C. -W. Qiu, J. K. W. Yang, *Nano Lett.* **14**, 4023-4029 (2014).

[2] H. Kim, J. Ge, J. Kim, S. Choi, H. Lee, H. Lee, W. Park, Y. Yin, S. Kwon, *Nat. Photonics* **3**, 534-540 (2009).

[3] A. S. Roberts, A. Pors, O. Albrektsen, S. I. Bozhevolnyi, *Nano Lett*. **14**, 783-787 (2014).

[4] J. S. Clausen, E. Højlund-Nielsen, A. B. Christiansen, S. Yazdi, M. Grajower, H. Taha, U. Levy, A. Kristensen, N. A. Mortensen, *Nano Lett*. **14**, 4499-4504 (2014).

[5] T. Xu, Y. -K. Wu, X. Luo, L. J. Guo, *Nat. Commun*. **1**, 59 (2010).

[6] Y. -W. Huang, W. T. Chen, W. -Y. Tsai, P. C. Wu, C. -M. Wang, G. Sun, D. P. Tsai, *Nano Lett.* **15**, 3122-3127 (2015).

[7] H. Hu, Q. -W. Chen, J. Tang, X. -Y. Hu, X. -H. Zhou, *J. Mater. Chem.* **22**, 11048 (2012).

[8] Y. Cui, I. Y. Phang, Y. H. Lee, M. R. Lee, Q. Zhang, X. Y. Ling, *Chem. Commun.* **51**, 5363-5366 (2015).

[9] P. Vukusic, J. R. Sambles, C. R. Lawrence, R. J. Wootton, *Nature* **410**, 36 (2001).

[10] S. Kinoshita, S. Yoshioka, J. Miyazaki, *Rep. Prog. Phys.* **71**, 076401 (2008).

[11] M. A. Kats, R. Blanchard, P. Genevet, F. Capasso, *Nat. Mater.* **12**, 20-24 (2013).

[12] Z. Li, S. Butun, K. Aydin, *ACS Photonics* **2**, 183-188 (2015).

[13] C. S. Park, V. R. Shrestha, S. S. Lee, E. S. Kim, D. Y. Choi, *Sci. Rep.* **5**, 8467 (2015).

[14] S. S. Mirshafieyan, J. Guo, *Opt. Express* **22**, 31545-31554 (2014).

[15] K. Mao, W. Shen, C. Yang, X. Fang, W. Yuan, Y. Zhang, X. Liu, *Sci. Rep.* **6**, 19289 (2016).

[16] C. H. Park, Y. T. Yoon, S. S. Lee, *Opt. Express* **20**, 23769-23777 (2012).

[17] B. Zeng, Y. Gao, F. J. Bartoli, *Sci. Rep*. **3**, 2840 (2013).

[18] V. R. Shrestha, S. S. Lee, E. S. Kim, D. Y. Choi, *Nano Lett.* **14**, 6672-6678 (2014).

[19] X. Zhu, C. Vannahme, E. Højlund-Nielsen, N. A. Mortensen, A. Kristensen, *Nat. Nanotech.* **11**, 325-329 (2016).

[20] F. Cheng, J. Gao, T. S. Luk, X. Yang, *Sci. Rep.* **5**, 11045 (2015).

[21] K. Kumar, H. Duan, R. S. Hegde, S. C. W. Koh, J. N. Wei, J. K. W. Yang, *Nat. Nanotech.* **7**, 557-561 (2012).

[22] C. Yang, W. Shen, J. Zhou, X. Fang, D. Zhao, X. Zhang, C. Ji, B. Fang, Y. Zhang, X. Liu, L. J. Guo, *Adv. Opt. Mater*. **4**, 1981-1986 (2016).

[23] L. Duempelmann, A. Luu-Dinh, B. Gallinet, L. Novotny, *ACS Photonics* **3**, 190-196 (2016).

[24] K. T. Lee, J. Y. Jang, S. J. Park, C. Ji, S. M. Yang, L. J. Guo, H. J. Park, *Adv. Opt. Mater*. **4**, 1696-1702 (2016).

[25] J. Proust, F. Bedu, B. Gallas, I. Ozerov, N. Bonod, *ACS Nano* **10**, 7761-7767 (2016).

[26] S. C. Yang, K. Richter, W. J. Fischer, *Appl. Phys. Lett.* **106**, 081112 (2015).

[27] W. Yue, S. Gao, S. S. Lee, E. S. Kim, D. Y. Choi, *Sci. Rep.* **6**, 29756 (2016).

[28] N. Meinzer, W. L. Barnes, I. R. Hooper, *Nat. Photonics* **8**, 889-898 (2014).

[29] D. Lin, P. Fan, E. Hasman, M. L. Brongersma, *Science* **345**, 298-302 (2014).

[30] K. Seo, M. Wober, P. Steinvurzel, E. Schonbrun, Y. Dan, T. Ellenbogen, K. B. Crozier, *Nano Lett.* **11**, 1851-1856 (2011).

[31] M. Khorasaninejad, N. Abedzadeh, J. Walia, S. Patchett, S. S. Saini, *Nano Lett.* **12**, 4228-4234 (2012).

[32] N. Dhindsa, S. S. Saini, *J. Appl. Phys.* **117**, 224302 (2015).[33] Y. F. Yu, A. Y. Zhu, R. Paniagua-Domínguez, Y. H. Fu, B. Luk'yanchuk, A. I. Kuznetsov, *Laser Photon. Rev*. **9**, 412-418 (2015).

[34] I. Staude, A. E. Miroshnichenko, M. Decker, N. T. Fofang, S. Liu, E. Gonzales, J. Dominguez, T. S. Luk, D. N. Neshev, I. Brener, Y. Kivshar, *ACS Nano* **7**, 7824-7832 (2013).

[35] R. G. Kuehni, *Color: An Introduction to Practice and Principles* (John Wiley & Sons, 2012), pp. 73-75.

[36] E. H. Cho, H. S. Kim, J. S. Sohn, C. Y. Moon, N. C. Park, Y. P. Park, *Opt. Express* **18**, 27712-27722 (2010).

[37] Y. S. Do, J. H. Park, B. Y. Hwang, S. -M. Lee, B. -K. Ju, K. C. Choi, *Adv. Opt. Mater.* **1**, 133-138 (2013).

[38] Lumerical Solutions Inc., "FDTD Solutions," https://www.lumerical.com/tcad-products/fdtd/.

[39] P. Spinelli, M. A. Verschuuren, A. Polman, *Nat. Commun.* **3**, 692 (2012).

[40] J. van de Groep, A. Polman, *Opt. Express* **21**, 26285-26302 (2013).

[41] A. I. Kuznetsov, A. E. Miroshnichenko, Y. H. Fu, J. B. Zhang, B. Luk'yanchuk, *Sci. Rep.* **2**, 492 (2012).

[42] P. Moitra, B. A. Slovick, W. Li, I. I. Kravchencko, D. P. Briggs, S. Krishnamurthy, J. Valentine, *ACS Photonics* **2**, 692-698 (2015).

Figure 1. (a) Configuration of the proposed subtractive color filters incorporating a metasurface that is comprised of an array of c-Si NPs, which is integrated with a combination of nanostructured DM and HM in Al. Three primary subtractive colors of cyan, magenta, and yellow are produced in response to normally impinging white light. (b) Nanofabrication procedure employed for manufacturing the device.

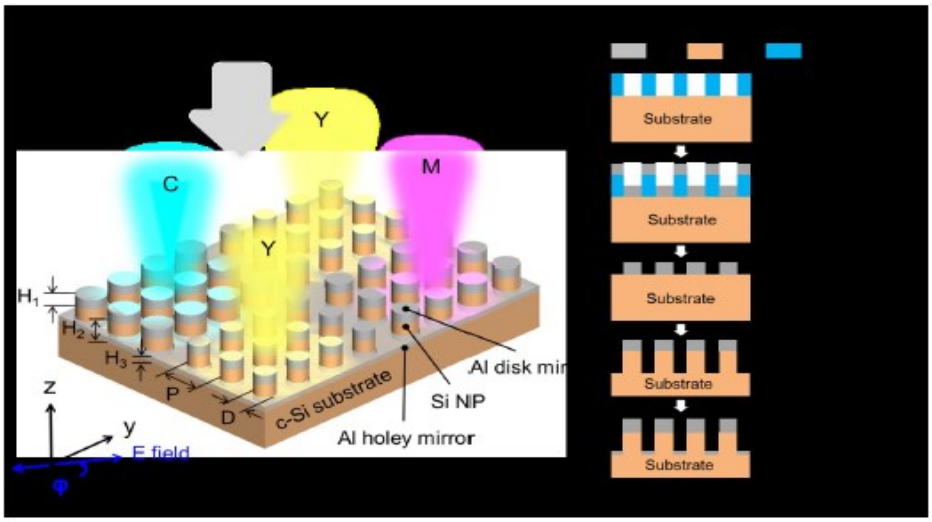

Figure 2. (a) SEM images of the completed filters of CMY colors for which the NP diameter is chosen to be D = 140, 115 and 90 nm for a constant period of P = 240 nm, respectively. The insets include the individual bright-field microscope images relating to the prepared devices with a footprint of 30 µm × 30 µm. (b) Measured and simulated optical reflection spectra and (c) corresponding chromaticity coordinates in the CIE 1931 chromaticity diagram.

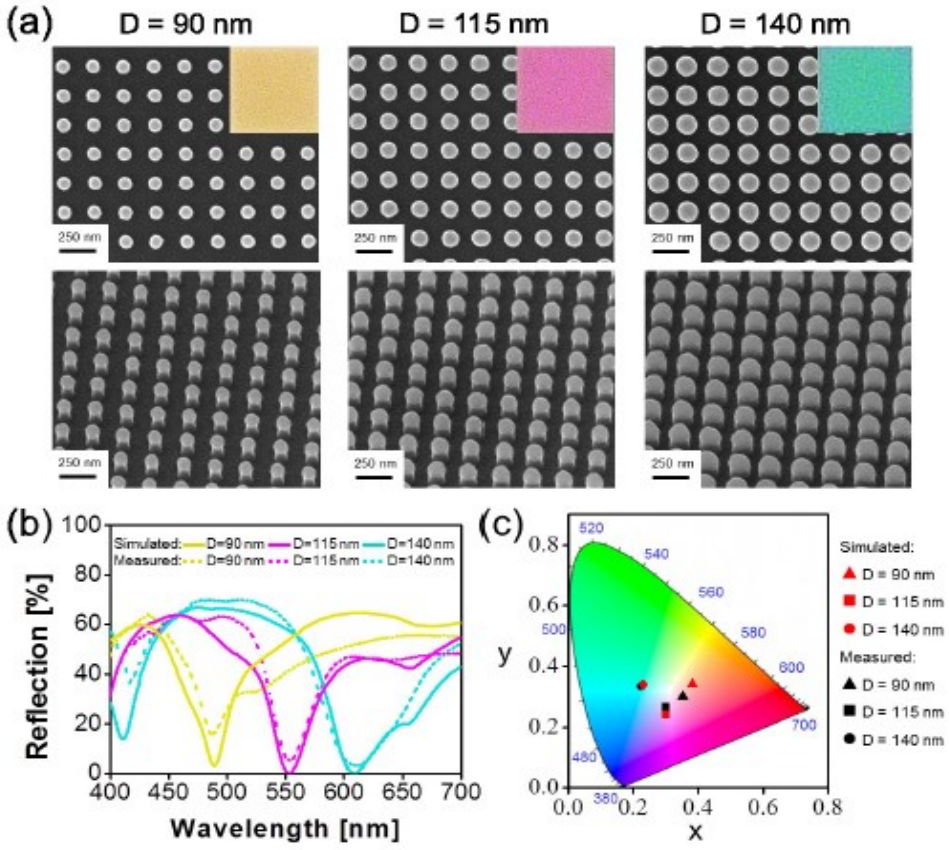

Figure 3. (a) Simulated and measured reflection spectra of the proposed color filters for which the NP diameter ranges from D = 90 to 160 nm at a constant period of P = 240 nm, with the location of the reflection dips traced by the dashed line. The insets in the measured spectra show the observed bright-field microscope images corresponding to a footprint of 30 µm × 30 µm. (b) Chromaticity coordinates in response to the spectra when the evolution of the color output with increasing NP diameter is indicated by the black arrow.

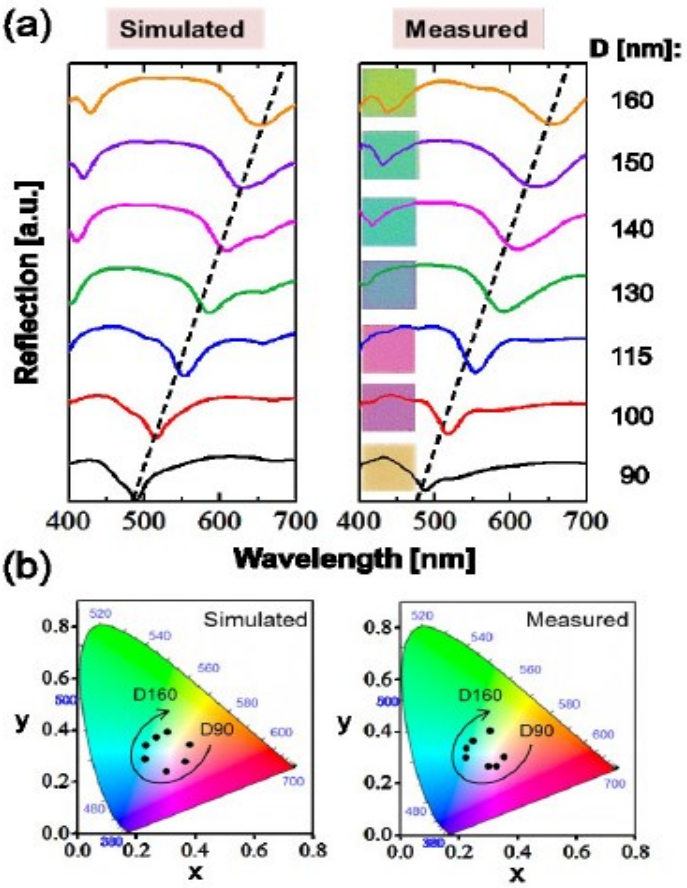

Figure 4. Contour map of (a) the simulated and (b) the measured reflection spectra for the magenta filter as a function of the incident angle θ for the TM and TE polarizations, respectively.

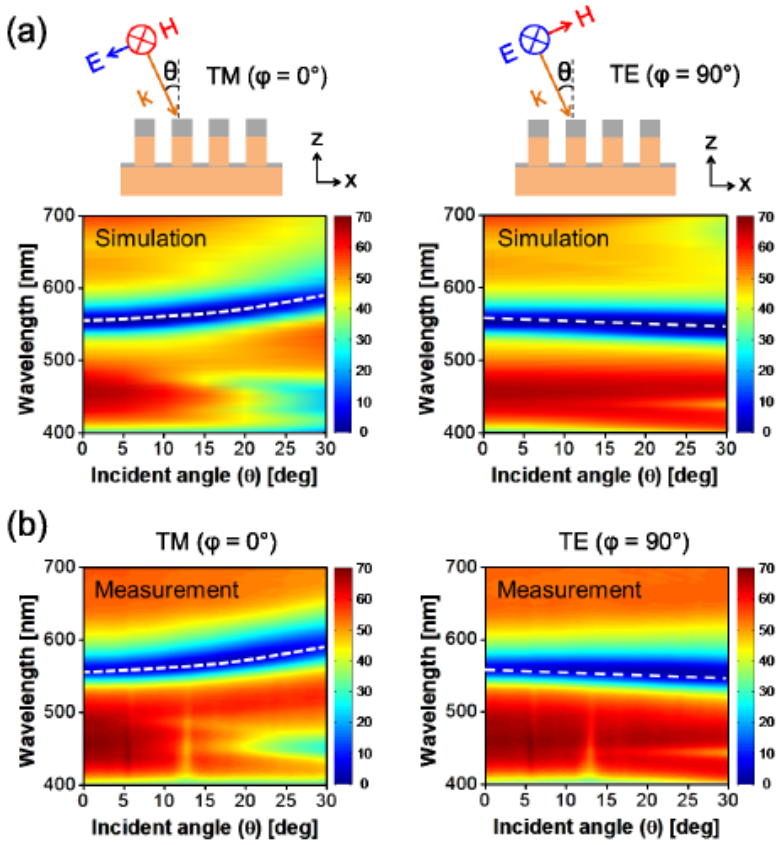

Figure 5. (a) Simulated reflection spectra for the proposed magenta color filter, with the NP diameter of D = 115 nm, where the resonance dip is located at λ = 552 nm. (b) Normalized E- and H-field profiles at resonance. The excitation of an MD resonance mode is verified through an enhanced H-field and corresponding E-field loop in the middle and vicinity of the Si NP, respectively.

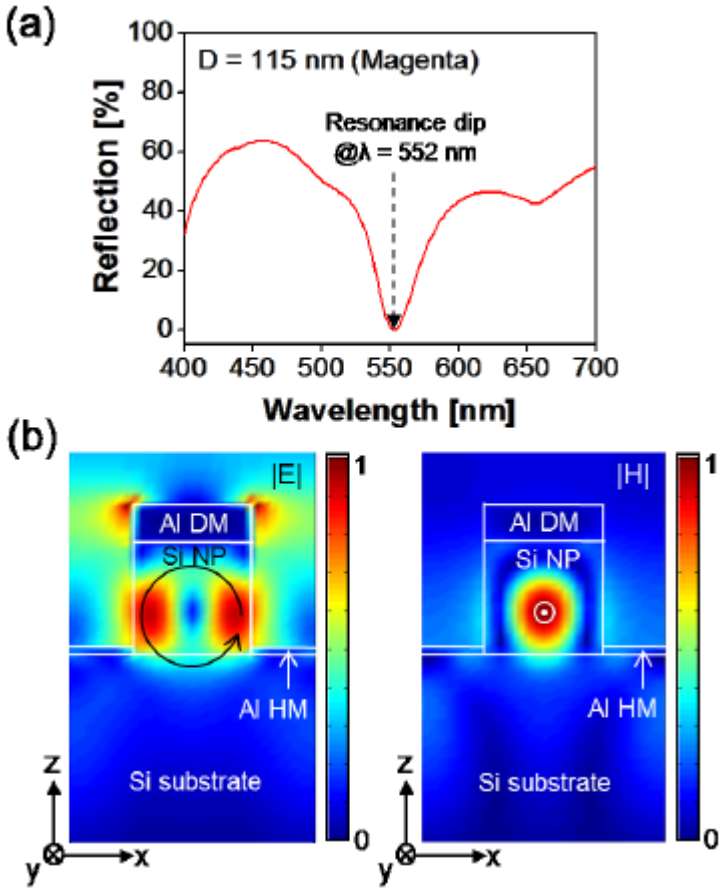

Figure 6. (a) Calculated reflection spectra and (b) normalized E- and H-field profiles for the NP structures depending on the presence of the nanostructured DM and the HM.